Title
STRUCTURE AND PROPERTIES OF Fe-Ni-Co-Ti VARAGING STEEL

Authors
Cheng, I-Lin
Thomas, G.

Publication Date
1967-09-01

UCRL-17803

c.2

University of California

Ernest O. Lawrence Radiation Laboratory

STRUCTURE AND PROPERTIES OF Fe-Ni-Co-Ti MARAGING STEEL

I-Lin Cheng and G. Thomas

September 1967

Berkeley, California

DISCLAIMER

Submitted to Trans. ASM

UCRL-17803
Preprint

UNIVERSITY OF CALIFORNIA
Lawrence Radiation Laboratory
Berkeley, California

AEC Contract No. W-7405-eng-48

STRUCTURE AND PROPERTIES OF Fe-Ni-Co-Ti MARAGING STEEL

I-Lin Cheng and G. Thomas

September 1967

STRUCTURE AND PROPERTIES OF Fe-Ni-Co-Ti MARAGING STEEL

I-Lin Cheng and G. Thomas

Inorganic Materials Research Division, Lawrence Radiation Laboratory,
and Department of Mineral Technology, College of Engineering,
University of California, Berkeley, California

September 1967

ABSTRACT

The structure of a relatively simple maraging alloy has been investigated by electron metallography and x-ray analysis in order to identify microstructural features and their relation to mechanical properties.

The as-quenched martensite is lath-shaped and heavily dislocated. Upon aging, plate-shaped precipitates of Ni_3Ti are formed together with reversion to austenite and a decrease in dislocation density. At high stresses these precipitates are observed to deform with the matrix. It is concluded that precipitation hardening is the main strengthening mechanism. Grain boundary precipitation is thought to be the cause of intergranular embrittlement. Precipitation of Ti compounds with C, N, O was also detected.

The orientation relationships between matrix and $\eta(Ni_3Ti)$ were found to be $(0001)_\eta // (110)_\alpha$ and $[2\bar{1}\bar{1}0]_\eta // [1\bar{1}1]_\alpha$.

INTRODUCTION

Because of their superior high strength (1), ductility (1), high temperature creep resistance (2) and low temperature properties (3), maraging steels have become one of the most promising materials for structural purposes.

A high nickel, low carbon, alloy steel, when annealed and quenched, can produce a relatively soft (R_c25) and ductile BCC martensite. Upon reheating or aging, intermetallic compounds, instead of carbides, precipitate out from the supersaturated solution and precipitation hardening is thought to be the major hardening mechanism (4,5). Recently, Mihalisin (6) utilized neutron diffraction analysis and suggested that ordering might also play a role in strengthening.

Here, a Fe-Ni-Co-Ti maraging steel was studied in order to limit complications due to compositional variables. The cobalt content is higher than is usual for maraging steels (23.6 wt%) and possible benefits from this were investigated. The changes in microstructures with mechanical properties were related. The orientation relationship between the matrix and precipitates was determined using selected area electron diffraction of the thin foils. Identification of the precipitates was done by electron diffraction and by using an electron microprobe analyzer and x-ray microanalyzer on overaged samples.

EXPERIMENTAL

The material used for this study was supplied by International Nickel Company as a hot rolled bar. The chemical composition is: Ni, 20.3 wt%; Co, 23.6 wt%; Al, 0.068 wt%; Ti, 0.17 wt%; C, 0.055 wt%; and Fe, the balance.

The bar was hot rolled with intermediate annealing down to 25 mils. Further reduction to produce foils suitable for electron microscopy work was done by cold rolling to 10 mils thickness.

The samples were vacuum-sealed in quartz tubes and solution-treated at 2100°F for 4 hours. Four different cooling rates were used, namely, furnace, water, air and liquid nitrogen. The M_s temperatures were determined by a differential thermal technique. Aging treatments were performed at 700°F and 900°F on all of the four differently quenched specimens.

Rockwell hardness was measured for each as-quenched and aged sample, and tensile tests were carried out on an Instron machine with a cross head speed of 0.05 cm/min.

Specimens prepared for optical microscopy were mechanically polished with emery papers and etched in acid ferric chloride. Extraction replicas were prepared by depositing carbon on etched specimens (etchant 15 mml HCl, 10 mml acetic acid, 10 mml HNO_3, and a few drops of glycerine) and removing the carbon film by subsequent etching. Thin foils for electron microscope were prepared by chemical and electro-polishing. 10 mil specimens were chemically thinned in a H_2O_2-H_3PO_4 bath to about 3 mils. Electropolishing was performed utilizing the "window" method in an electrolyte of 90% glacial acetic acid and 10% perchloric acid with an applied voltage of about 20 V DC. All the replicas and thin foils were observed in a Siemens Elmiskop IA microscope with an operating condition of 40 kV for x-ray XMA microanalysis and 100 kV for replicas and thin foils.

In addition to the electron microscopy, x-ray analysis was performed on aged samples using an XRD-3 diffractometer with vanadium filtered chromium Kα radiation in order to estimate the amount of austenite produced upon aging. Finally, electron microprobe analysis was done on overaged alloys using a MAC model 400 analyzer.

RESULTS AND DISCUSSION

Transformation Temperature

The range of ferrite austenite-transformation temperature α-γ, or As-A_f, as determined by the differential thermal method, was found to be 1400°F-1620°F, and the martensite transformation temperature 690°F-540°F. The latter was obtained on furnace cooled samples at a cooling rate of about 4.8°C/min. Since it has been found that cooling rates had no significant effect on the M_s temperature for the Fe-Ni alloys (7), it is concluded that M_s temperatures do not differ appreciably from one another by the four kinds of quenching studied.

As-Quenched State

All the quenched samples after different cooling rates showed an equiaxed structure by optical microscopy and typical lathlike dislocated martensite by electron micrographs (Fig. 1). No internal twinning was observed in martensite. This is consistent with the fact that the M_s temperature of this alloy is high (8).

In the electron micrographs, the martensite "laths" appear to be parallel with slight misorientation. Bundles of these laths are thought to produce the blocky structure often referred to as "massive martensite" (9) as seen in the optical micrograph. Some of the martensite laths were twin related as can be detected from the select area diffraction pattern from two adjacent grains.

There were no substantial differences in the quenched structure among these four treatments, except the liquid nitrogen cooling specimen showed narrower martensite laths which might be responsible for the higher hardness and yield stress observed after this treatment (Fig. 2 and Table 1). The strength of the as-quenched martensite is due, principally, to the solid solution hardening combined with the work hardening contributions from transformation substructure (10,11), whilst their high ductility produced is presumably due to the low carbon content, the absence of any precipitates,* and the high dislocation density.

The strength of the present martensite (contains 23.6% Co) is about the same as that of more conventional maraging steels (1) containing 5-7% Co. It appears, therefore, that cobalt in solid solution does not have a strong strengthening effect. Mihalisin (6) has proposed that cobalt may effect ordering of the solid solution, but no evidence for this has been obtained in the present investigation, even after aging treatments, i.e. no superlattice reflections nor superlattice dislocations were resolved. Furthermore, the stress-strain curve for martensite (Fig. 3) is not what is expected for an ordered alloy.

The orientation relationship between martensite and austenite could not be obtained because of the relatively small amount of austenite remaining after quenching, as revealed by x-ray diffraction analysis (see Table 4).

Finally, the "burst" formation of martensite needles could be revealed

---

* No precipitation was detected in as-quenched martensitic structures, even after many attempts to detect them using dark field techniques.

TABLE 1. Tensile Properties*

Treatment (2100°F/4 hr Annealing)	Yield (0.2%) Ksi	Ultimate Ksi	Elongation %
LN As-Quenched	107	132	6.1
LN 700°F/$\frac{1}{4}$ hr	150	175	5.0
LN 700°F/1 hr	166	185	2.7
LN 700°F/3 hr	192	192	2.0
LN 700°F/12 hr+			
WC As-Quenched	98	112.2	7.2
WC 700°F/$\frac{1}{4}$ hr	147	164.5	4.8
WC 700°F/1 hr	162	177.5	3.6
WC 700°F/3 hr	168	186	2.2
WC 700°F/12 hr+			
FC As-Quenched	96	114	6.5
FC 700°F/$\frac{1}{4}$ hr	120	137.5	5.2
FC 700°F/1 hr	145	151	4.1
FC 700°F/3 hr	153	160	2.9
FC 700°F/12 hr+			
AC As-Quenched	97.5	120	6.2
AC 700°F/$\frac{1}{4}$ hr	131	140	4.9
AC 700°F/1 hr	147	156	3.9
AC 700°F/3 hr	155	163	2.7
AC 700°F/12 hr+			

[*] All the 900°F aging specimens broke before yielding.

[+] Broken before yielding.

from the differential temperature curves in the transformation temperature determination which showed serrated peaks as the M_s temperature was reached.

Aged State

Mechanical Properties

The changes of properties resulting from different aging conditions were measured at room temperature and the results are shown in Table 1 and Figs. 2 and 3. It is seen from Fig. 2 that the hardness increases very rapidly and the form of hardness-time curves follows those of precipitation hardening alloys, i.e., maximum hardness occurs at longer times as the aging temperature is lowered (700°F vs 900°F). The yield and ultimate tensile strength increase, but these are accompanied by a loss in ductility, as shown in Fig. 3. Also, the suggested typical maraging treatment (1) (3 hr age at 900°F), was not suitable for this alloy, since all the specimens given the 900°F aging treatment failed in a brittle manner with an intergranular fracture before yielding. This phenomenon will be discussed in association with the microstructural changes. Higher work hardening rates were also observed from the stress-strain curves (Fig. 3) as the aging progresses.

Identification of Precipitates

Qualitative chemical analysis by x-ray microanalysis and electron beam probe showed that the precipitate is composed of nickel and titanium. When examined on the electron microscope using x-ray microanalysis, the extracted precipitates show an Ni peak when mounted on a Ti grid and a Ti peak when mounted on an Ni grid (see Fig. 4).* Also, in Fig. 5, it is seen that in the overaged conditions the precipitates grow into a size which is detectable in the optical microscope and the electron beam probe x-ray image using TiK_α showed some agglomerates of Ti. In this case, due to the limitations imposed by the thickness of precipitates and penetration of the electron beam, the Ni content of the precipitate could not be determined because Ni together with Fe + Co is the abundant element in the matrix.

Fig. 6a shows an electron micrograph of a carbon extraction replica from a sample overaged at 600°C for 19-1/2 hrs, which showed a Rockwell hardness of only R_c24. Compared with the thin foil micrograph in Fig. 6b, the larger plates are probably the precipitates along former martensite boundaries, the rest being distributed uniformly throughout the matrix. During overaging, some austenite was detected in the micrographs. The austenite particles appear as small dots on the replica micrograph (Fig. 6a), and can be identified by selected area electron diffraction, as shown in Fig. 7.

After examining many foils and extraction replicas, the "d" spacings were obtained from the selected area diffraction patterns in the usual way and are shown in Table 3. Comparing these data with the x-ray powder data for Ni_3Ti yields a reasonable match. The precipitates are thus tentatively identified within the limits of electron diffraction as the Ni_3Ti hexagonal phase with the DO_{24} structure.

---

* The XMA was calibrated before analyzing the precipitates by mounting different foils in the analyzer. The calibration data is given in Table 2.

TABLE 2. Calibration Data for the XMA

(The emission lines of the metals listed below were excited with the continuous x-radiation of a Pt target and were monochromatized with a Li-F crystal.)

X-Ray Unit Voltage-Current KV-MA	"Z"	Element	Peak Position		Resolution (%)**	Peak Width 1/2 Max. Intern (Kev)
			Theoretical K_a	Experimental*		
40-5	22	Ti	4.51	4.42	20.3	0.90
35-1	26	Fe	6.40	6.41	17.2	1.10
30-1	27	Co	6.93	6.96	16.4	1.14
35-1	28	Ni	7.48	7.56	15.3	1.16
26-1	28	Ni***	7.48	7.44	17.5	1.30
50.5	40	Zr	15.77	15.90	11.1	1.76

* To obtain the energy from a peak position on the PHA, the scale is so calibrated that one reads the volts on the discriminator (0-100 volts) and multiplies by 0.2.

** Defined as $\frac{(\Delta V) \text{ at } 1/2\ I_{max}}{V \text{ at } I_{max}} \times 100.$

*** No monochromator.

TABLE 3. Interplanar Spacings of the Precipitates
(2100/4 hr Annealing, LN cooling, 600°C/19-1/2 hr aged)

Thin Film		Replica (Ring Patterns)	Austenite[†]	Martensite	Ni_3Ti[§]		
d(Å)	I/I_o[*]	d(Å)	d(Å)	d(Å)	d(Å)	I/I_o	(hkℓ)
2.21	M	2.21			2.21	20	200
2.14	M	--			2.13	50	201
2.075	S	--	2.08	2.027	2.07	50	004
1.943	VS	1.95			1.95	100	202
1.83	M	--		1.83			
--		--			1.72	20	203
--		--			1.54	10	122
--		--		1.43	1.51	20	204
1.35	M	--	1.37		1.330	20	205
1.26	S	1.273			1.276	50	220
1.16	M	1.16		1.17	1.173	20	206
1.09	M		1.09		1.095	10	401
--		--			1.087	50	224
1.06	M	1.06			1.068	50	402
--		--			1.046	20	207
1.032	W	--			1.038	20	008
--		--		1.013	1.027	20	403
0.973	W	--			0.974	10	404
0.94	W	0.94			0.940	10	226,412
--		--		0.906	0.920	10	405
0.85	W	0.85	0.85		0.831	10	421
--		--			0.819	20	422
--		--			0.800	10	423
0.775	W	--			0.779	10	505,414

---

[*] VS (very strong), S (strong), M (medium), W (weak).

[†] By x-ray diffraction.

[§] ASTM x-ray powder data file.

In some cases, rectangular particles were extracted and these particles were tentatively identified as TiC or TiN by means of their selected area diffraction patterns. The crystal structures of TiC and TiN are identical and they have similar lattice parameters, so, as Reisdorf has suggested (12), Ti (C,N) is used to indicate this compound. In a few replicas, oxides of titanium were also identified by electron diffraction.

Observations of the Maraging Structure

Observations of the maraged structure were done exclusively by electron microscopy, since no evidence of precipitation and only dark etching along the grain boundaries were observed in the optical microscope.

700°F Aging

During the early stage of aging, e.g., 15 minutes, no precipitation could be detected in bright field micrographs. However, in the diffraction pattern, faint streaks through the matrix diffraction spots were observed, which may indicate plate-like or disc-shaped "precipitates" with the streaking direction perpendicular to the plane of the particles. This is quite reasonable, since it is often possible to detect the evidence of solute atom clustering or G.P. zones in the diffraction patterns before a precipitate can be easily seen in the microstructure. No strain contrast could be revealed in the photographs, probably because the strain contrast is too small to be resolved and because of complexities from the incoherent scattering due to the high dislocation density. After the 3 hours aging treatment, small particles could be detected in the bright field image, but they were rather obscure because of the high dislocation density. However, in the dark field image produced by gun tilting, the presence of precipitates is quite obvious as Fig. 8 shows. The precipitates have an average diameter of about 180-200Å. The precipitates are uniformly distributed throughout the matrix, which suggests that they may have formed heterogeneously from the dense dislocation structure produced during the martensitic transformation. The precipitates begin to grow, having definite orientations and having a tendency to segregate on the martensite subboundaries in an aging time of 12 hours (as compared to 3 hours previously). The precipitates become larger at longer aging times. Because martensite boundaries and grain boundaries provide better sites for the precipitation, boundary precipitation occurs and boundary particles grow much larger than those in the matrix. These effects are more pronounced at higher aging temperatures (see Fig. 9).

900°F Aging

Aging for 1 hour at this temperature caused extensive subgrain boundary precipitation along the original martensite lath boundaries, as shown in Fig. 9. Aging for 3 hours, which is the suggested typical treatment, produced both matrix and boundary precipitation, although the boundary precipitates grow faster than those in the matrix. Dark field photomicrographs, as shown in Fig. 10, indicate the size and direction of the matrix precipitates, while the boundary precipitates usually lie in the plane of the boundaries. Twelve hours aging at this temperature caused some formation of subgrains due to recovery and recrystallization besides growth of precipitates.

Morphology of Precipitates and Their Orientation Relationship with the Matrix

Because of streaking in the diffraction pattern (e.g., Fig. 11), it is seen that the shape of the precipitate is either disc-like or plate-like (due to relaxation of the Laue diffraction conditions in one dimension). This is confirmed in the micrographs shown in Fig. 10, where the projections of the precipitates on (110) plane show rectangular shapes. The results have shown conclusively that the Ni_3Ti phase forms as plates and not needles as has been suggested (13). At the earliest stages the electron diffraction patterns show that the streaks are always straight lines, even for precipitates inclined in the foil. If the particles were rod-shaped, then the intensity is distributed as a disc and would give rise to curved streaks for all particle orientations other than those lying normal to the incident beam, as has been shown for precipitates in the Al-Mg_2Si system (14). Furthermore, on overaging, both foils and extraction replicas show the plate character of the precipitates unambiguously.

Analysis of the diffraction patterns showed that the precipitates lie on {110} planes of the matrix and have the expected orientation relationship, viz., $(0001)_\eta // (110)_\alpha$ and $[2\bar{1}\bar{1}0]_\eta // [1\bar{1}1]_\alpha$. An example is shown in Fig. 11 and confirms the earlier work of Pitter and Ansell (15) and Garwood and Jones (13).

Reversion of Austenite

The amount of austenite was determined by x-ray analysis using the formula (16):

$$\text{volume \% austenite} = \frac{100}{1 + (1.7)\left(\frac{I\alpha}{I\gamma}\right)}$$

where $I\alpha$ = integrated intensity of (200-002) martensite x-ray line

$I\gamma$ = integrated intensity of (200) austenite line.

The value of "1.7" was calculated as shown in the Appendix.

The results are given in Table 4. It is seen that upon aging the amount of austenite gradually increases. This phenomenon is thought to be due to the reversion of the metastable BCC phase to the equilibrium austenite and ferrite phases due to the depletion of Ni from the matrix as a result of precipitation.

Overaging by aging at 1100°F for 19.5 hours caused softening of this alloy (R_c25). This phenomenon is related with the amount of austenite present which is rather high (39.4%). Examination of replicas and thin foils of the overaged specimen revealed small particles which were determined to be austenite by electron diffraction analysis (e.g. Fig. 7). Hence, it was concluded that overaging occurred primarily because of austenite reversion (with a concurrent slight growth of precipitates). There appears to be a critical amount of austenite at which the softening occurs.

Structural Changes and Mechanical Properties

The high ductility observed in the as-quenched state is thought to be related to the low carbon content (which eliminates the brittleness characteristic which exists in plain carbon steels), and the high dislocation density introduced during transformation.

In these experiments, it was found that the ductility decreased with aging time and/or temperature. Careful examination of the substructures showed that there was a strong tendency for grain boundary precipitation to occur and this was associated with a marked decrease in the ductility

TABLE 4. Amount of Retained Austenite

Treatment	% Austenite
As-Quenched (LN)	1.5
700°F/$\frac{1}{4}$ hr	3.57
700°F/1 hr	8.34
700°F/3 hrs	8.93
700°F/12 hrs	14.15
900°F/$\frac{1}{4}$ hr	4.50
900°F/1 hr	9.05
900°F/3 hrs	13.30
900°F/12 hrs	27.00
1100°F/19.5 hrs	39.40

(e.g. 700°F/12 hrs aged specimen), as in Fig. 10. Also, some of the specimens broke in the grips which indicated a noticeable notch sensitivity. This brittleness has been suggested by Floreen and Speich (17) to be due to grain boundary embrittlement in the absence of Mo. They showed by carbon replica fractographs of the surfaces of fractured charpy bars that the molybdenum-containing alloy showed a dimpled-type fracture surface characteristic of ductile fracture, whereas the brittle titanium-containing alloy showed a flat fracture surface typical of a brittle intergranular fracture. This has been confirmed by fractography experiments (see Fig. 12).

Preferential precipitation along the boundaries, i.e., both grain boundaries and sub-boundaries, makes the boundaries stronger. Thus, the dislocations cannot easily cross the boundaries to continue the deformation and have a tendency to pile up against the boundaries until the internal stresses set up are large enough to break or shear the precipitates on the boundaries. This phenomenon is clearly shown in Fig. 13 where the bending and/or shearing of particles can be seen after 30% cold rolling. It is also interesting to note in Fig. 13b that fewer precipitates in the matrix are deformed compared to the boundary precipitates. The shearing directions of the precipitates are <111>, which are the slip directions in BCC metals.

In addition, the presence of Ti(C,N) particles may also be a factor causing low notch toughness of this alloy (18).

Strength of Maraging Steels

There are three factors which are thought to control the hardening mechanism, namely, dispersion hardening, ordering, and martensitic grain size. Another factor is the carbon content, which in the present alloy is rather small so that its contribution to hardening may be neglected as compared to the other parameters.

Dispersion of Precipitates

Several theories have been proposed to account for the yield stress of precipitation hardenable alloys (18). Orowan suggested that the plastic strain results from the expansion of dislocation loops surrounding particles which intersect the glide plane. Ansell and Lenel (19) suggested that detectable plastic flow would occur only when the particles are being sheared or broken by the passing dislocations. Dislocations pile up against second-phase particles and the particles rupture whenever the accumulated stress is large enough. These two theories will be tested separately as follows:

a. Orowan type:

The modified Orowan relationship is that the initial shear yield stress should be given by:

$$\tau = \tau_s + \frac{Gb}{4\pi} \phi \ln \left\{ \frac{d-2r}{2b} \right\} \frac{1}{(d-2r)/2} \qquad (1)$$

where G = shear modulus of the matrix = 7300 Kg/mm^2

τ_s = initial yield stress of the matrix; take the value of as-quenched state = 53,000 psi (37.3 Kg/mm^2)

b = Burgers vector = 2.49Å

r = mean particle radius = 90 ∿ 120Å

d = mean planar interparticle spacing = 400 - 500Å

$\phi = 1/2(1 + 1/1-\nu)$. ν = Poisson's ratio = 0.3. $\phi = 1.215$

The above values are based on the aging condition of 700°F/3 hrs, corresponding to peak hardness (Figs. 2, 8). Using the above values, we obtain $\tau = 140{,}000$ psi.

b. Ansel-Lenel type:

The final form of Ansell and Lenel's model is that the yield stress of a dispersion hardened material should be (20):

$$\tau = \tau_s + \frac{G'}{rC} \frac{f^{1/3}}{(0.82-f^{1/3})} \tag{1}$$

where τ_s = yield stress of the matrix; take τ_s = 53,000 psi as previously

G' = shear modulus of the Ti-Ni phase (21), 8.9×10^6 psi

C = a constant approximately equal to 30

f = volume fraction of particles approximately equal to 5.2% (for spherical particles $\frac{r}{R} + \frac{f^{1/3}}{0.82}$ where r is radius of particles and 2R is mean separation between particles).

Hence we obtain an initial yield stress of 110,000 psi.

Comparing the results from these two models with the experimental determination value, which showed a tensile yield stress of 192,000/2 psi* or shear yield of 96,000 psi, it is suggested that the Ansell's model may be the plausible one. Our observations of particle shearing also lend support to Ansell's model.

---

[*] By assuming that the tensile yield stress is about twice the shear stress.

The increasing work hardening rate occurring during the aging treatment (Fig. 3) is thought to be due to the resistance to dislocation motion by precipitates or by multiplication of dislocations as a result of dislocation precipitate interactions, as is typical of precipitation hardened systems (18).

Ordering

Although the precipitated phase Ni_3Ti (DO_3 or DO_{24}) is ordered, the matrix may also be ordered (20). In view of the composition of this alloy, Fe-Ni and Co may combine to form an ordered phase. Mihalisin (6), using neutron diffraction, did observe ordering of this type of alloy in which the ordered phase had a composition near Fe_2CoNi. In the present work, an attempt was made to find the existence of superdislocations which would indicate order (22), but no such evidence was found. Hence, the effect due to ordering of the matrix is probably very small, and there does not seem to be much benefit in using relatively large amounts of cobalt.

Martensitic Grain Size

It was observed in this alloy that after quenching in liquid nitrogen, the hardness and yield strength are higher than after other quenching methods. This was explained as due to the finer martensitic grain size as observed in the electron microscope, although no such tendency can be observed by light optical microscopy.

During subsequent aging, the dislocations annealed out gradually due to recovery, as was observed in the electron microscope and thus the contribution to strengthening from the dislocation density decreased as the precipitation hardening mechanism became more effective. Some contribution to the strength must also come from the transformation to austenite during aging.

CONCLUSIONS

1. The structures are relatively insensitive to cooling rates; a BCC lath-like dislocated martensite was produced in each case; and the cooling rate does not effect the M_s transformation temperature appreciably in this alloy.

2. The martensite platelets produced by quenching are relatively soft and contain a high dislocation density. Low carbon content and high dislocation density may be responsible for their ductility. There is no evidence for long range order in as-quenched martensite.

3. The precipitates were identified as Ni_3Ti, which is a hexagonal phase. The precipitates are formed as plates and are oriented with the martensite matrix such that $(0001)_\eta // (110)_\alpha$ and $[2\bar{1}\bar{1}0]_\eta // [1\bar{1}1]_\alpha$.

4. Grain boundary precipitation is the probable cause of brittleness of this alloy. The fractured surface showed an intergranular fracture. The existence of Ti(C,N) particles may be an additional factor in embrittling.

5. Grain boundary precipitates break or shear as the stress from the surrounding dislocation groups becomes large enough. Precipitates are sheared in the <111> slip directions of the matrix.

6. The strength of maraging steels is due primarily to dispersion hardening. No evidence was obtained for ordering in the matrix and it is suggested that little benefit is derived from using large amounts of cobalt.

7. Upon aging, the dislocation density decreases as a result of recovery,

and the amount of austenite formed increases with aging time and temperature.

8. Softening occurs when the amount of austenite exceeds a certain critical value. Overaging is thus due to reversion of austenite with little appreciable growth of precipitates.

9. Although high strength can be obtained in this alloy, it is not very promising because of its low ductility. Hence, the prevention of boundary precipitation, e.g., the beneficial addition of Mo, may improve the properties greatly.

ACKNOWLEDGMENTS

We wish to thank the United States Atomic Energy Commission for continued financial support. This work was done in partial fulfillment of the M.S. degree in the College of Engineering (I. Cheng). We acknowledge the assistance of Dr. E. Sturcken with the calibrations of the XMA attachment to the Siemens.

APPENDIX

Calculations of volume % austenite with negligible amounts of third phase, the volume percent of austenite is determined by:

$$\%\gamma = \frac{100}{1 + \frac{R\gamma}{R\alpha}\,\frac{I\alpha}{I\gamma}}$$

$$\frac{R\gamma}{R\alpha} = \frac{V\alpha^2 F\gamma^2 P\gamma[(1+\cos^2 2\theta)/(\sin^2\theta\cos\theta)]\gamma[\exp(-2m)]\gamma}{V\gamma^2 F\alpha^2 P\alpha[(1+\cos^2 2\theta)/(\sin^2\theta\cos\theta)]\alpha[\exp(-2m)]\alpha}$$

where F is the absolute value of the structure factor, P is the multiplicity factor, V is the volume of unit cell, exp(-2m) is the temperature factor and $\frac{1+\cos^2 2\theta}{\sin^2\theta\cos\theta}$ = Lorentz polarization factor.

Factor	Martensite (200-002)	Austenite (200)
2θ	106.2	79.4
θ	53.1	39.7
$\frac{1+\cos^2 2\theta}{\sin^2\theta\cos\theta}$	2.815	3.293
$\sin\theta/\lambda$	0.35	0.279
F^2	$4(14.62)^2$	$16(16.50)^2$
p	4+2	6
exp(-2m)	0.91	0.94
V^2	$(2.866)^4(2.873)^2$	$(3.557)^6$

The ratio $\frac{R\gamma}{R\alpha}$ is thus calculated from the above values: $\frac{R\gamma}{R\alpha} = 1.7$.

REFERENCES

1. R. F. Decker, J. T. Eash, and A. J. Goldman, 18% Nickel Maraging Steel, ASM Trans Quart, 55 (1962) 58.
2. S. Floreen and R. F. Decker, Maraging Steel for 100F Service, ASM Trans Quart, 56 (1963) 403.
3. R. H. Bush, Mechanical Properties of an Ausformed Maraging Steel, ASM Trans Quart 56 (1963) 885.
4. A. J. Baker and P. R. Swann, The Hardening Mechanism in Maraging Steels, ASM Trans Quart, 57 (1964) 1009.
5. G. P. Miller and W. I. Mitchell, Structure and Hardening Mechanisms of 18% Ni-Co-Mo Maraging Steels, J. Iron and Steel Inst., 203 (1965) 899.
6. J. R. Mihalisin, Age Hardening and Structure of Iron-Nickel-Cobalt Alloys, ASM Trans Quart, 59 (1966) 60.
7. A. Gilbert and W. S. Owen, Diffusionless Transformation in Iron-Nickel, Iron-Chromium and Iron-Silicon Alloys, Acta Met., 10 (1962) 45.
8. O. Johari and G. Thomas, Factors Determining Twinning in Martensite, Acta Met., 13 (1965) 1211.
9. G. P. Miller and W. I. Mitchell, Structure of Nickel-Cobalt-Molybdenum Maraging Steel in the Air-Cooled Condition, J. Iron and Steel Inst., 203 (1965) 895.
10. G. R. Speich and P. R. Swann, Yield Strength and Transformation Substructure of Quenched Iron-Nickel Alloys, J. Iron and Steel Inst., 203 (1965) 480.
11. O. Johari and G. Thomas, Structure and Strength of Ausformed Steel, ASM Trans Quart, 58 (1965) 563.

12. B. G. Reisdorf, Identification of Precipitates in 18, 20 and 25% Nickel Maraging Steels, ASM Trans Quart, 56 (1963) 783.

13. R. D. Garwood and R. D. Jones, Electron Microscope Study of the Structure of a 25% Ni, Ti, Al Maraging Steel, J. Iron and Steel Inst., 204 (1966) 512.

14. G. Thomas, Some Investigations of Precipitation, <u>Proc. of the Sixth International Congress for Electron Microscopy</u>, August 28 - September 4, 1966, Maruzen Co., Ltd., Nihonbashi, Tokyo, Japan (1966) 389.

15. R. K. Pitler and G. S. Ansell, Precipitation in High Nickel Maraging Steel, ASM Trans Quart, 57 (1964) 220.

16. H. R. Erard, Advances in X-Ray Analysis, ed. by W. M. Mueller <u>et al</u>., Plenum Press, New York (1963) 256.

17. S. Floreen and G. R. Speich, Some Observations of the Strength and Toughness of Maraging Steel, ASM Trans Quart, 57 (1964) 714.

18. A. Kelly and R. B. Nicholson, Precipitation Hardening, Prog. Mater. Sci., 10 (1963) 336.

19. G. S. Ansell, Fine Particle Effect in Dispersion-Strengthening, Acta Met., 9 (1961) 518.

20. C. G. Shull and S. Siegel, Neutron Diffraction Studies of Order-Disorder in Alloys, Phys. Rev. 75 (1949) 1008.

21. W. J. Buehler and R. C. Wiley, Ti-Ni Ductile Intermetallic Compound, ASM Trans Quart, 55 (1962) 269.

22. W. Bell, W. R. Roser and G. Thomas, Diffraction Analysis of Dislocation Pairs for Detecting Order in Solid Solutions, Acta Met., 12 (1964) 1247.

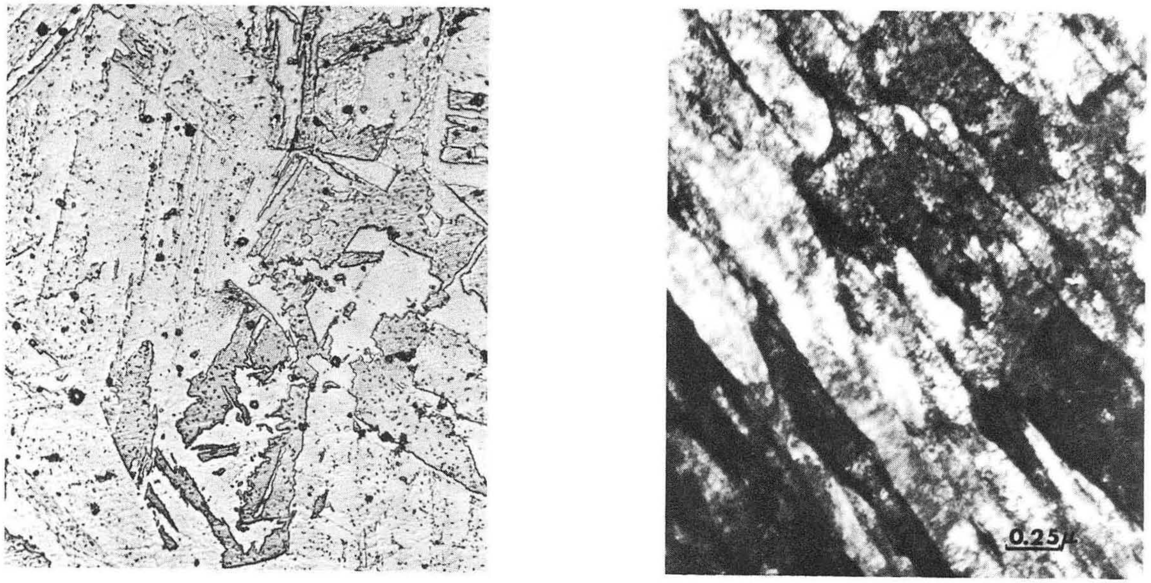

XBB 679-5312

Fig. 1 As-quenched states (2100°F annealing); (a) optical micrograph (water cooled), $FeCl_3$ etched, (b) martensite platelets in LN cooled state, showing high dislocation density.

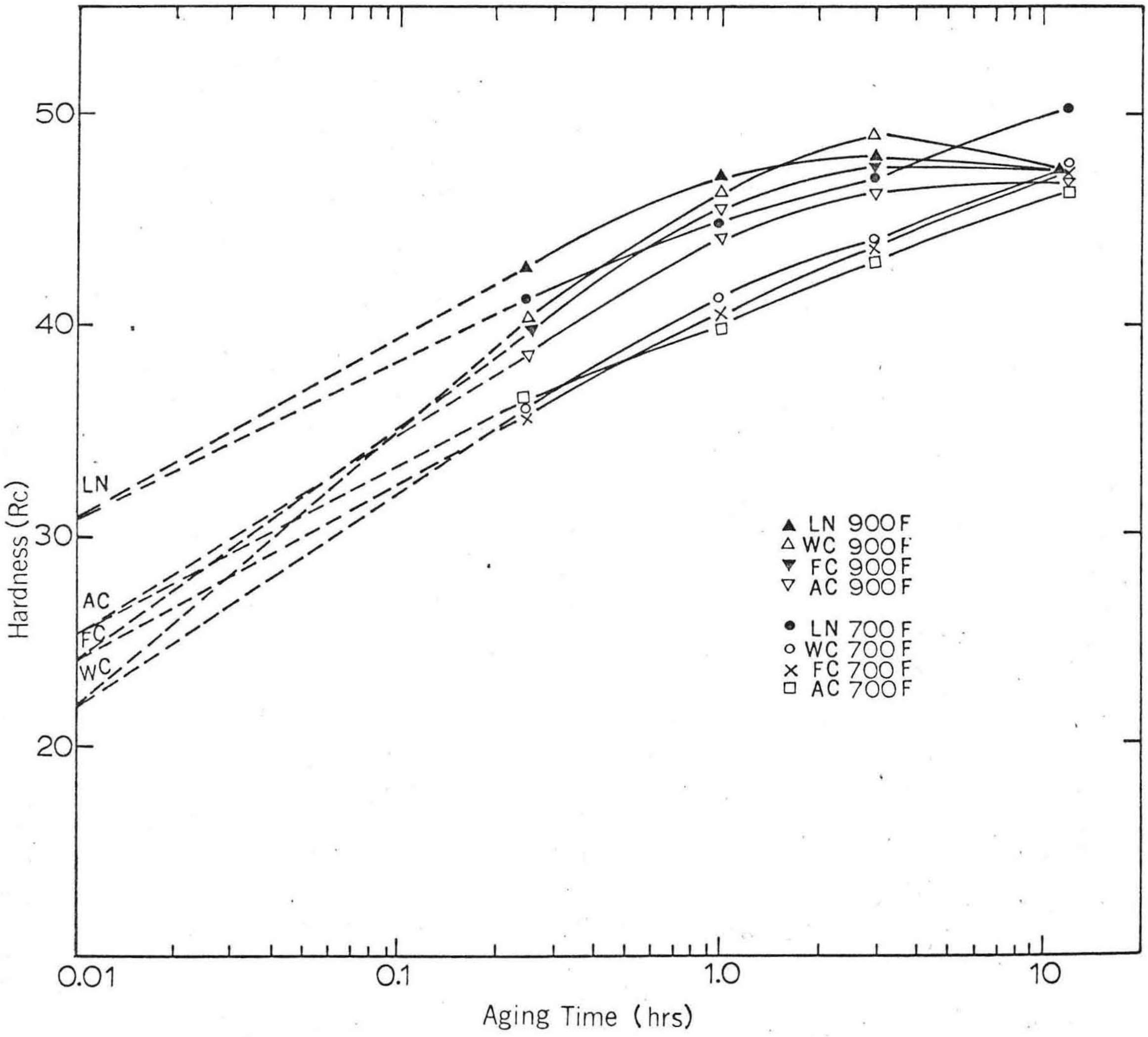

MUB-13761

Fig. 2 Hardness-aging time curves

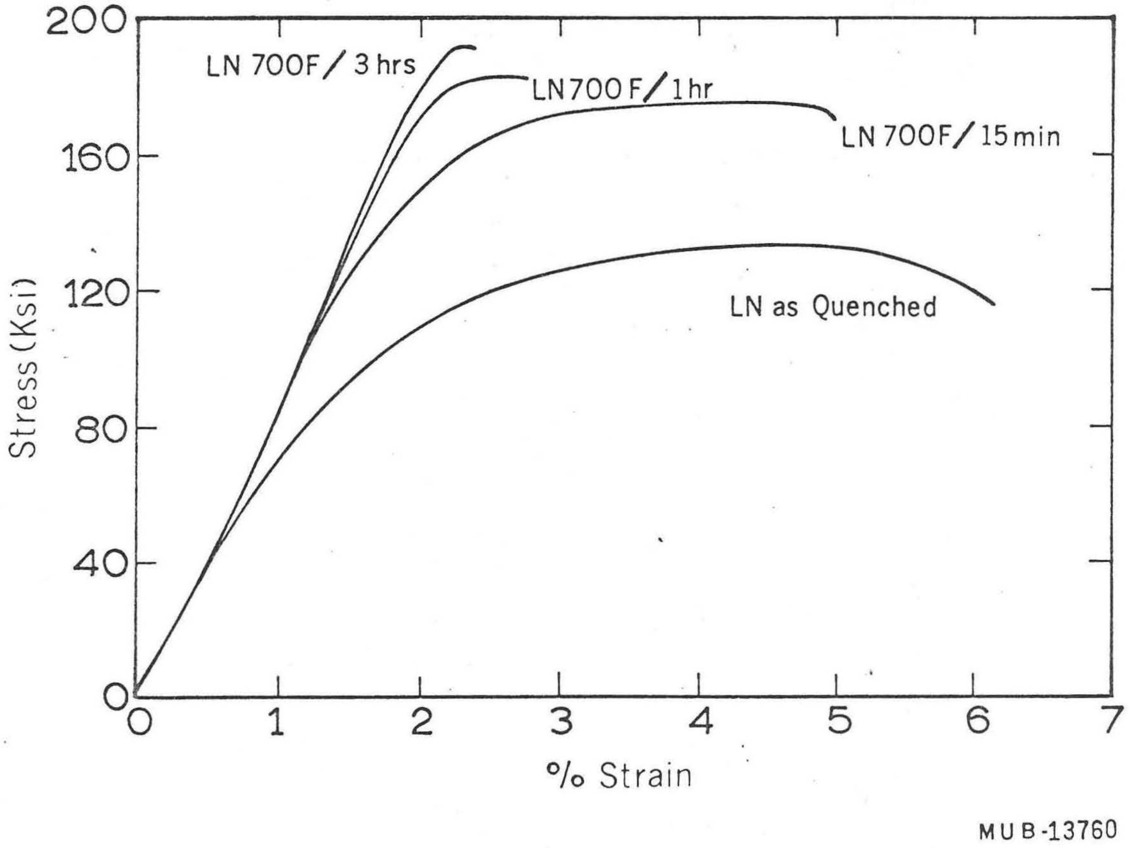

Fig. 3 Stress-strain curves of aged alloys after quenching in liquid nitrogen.

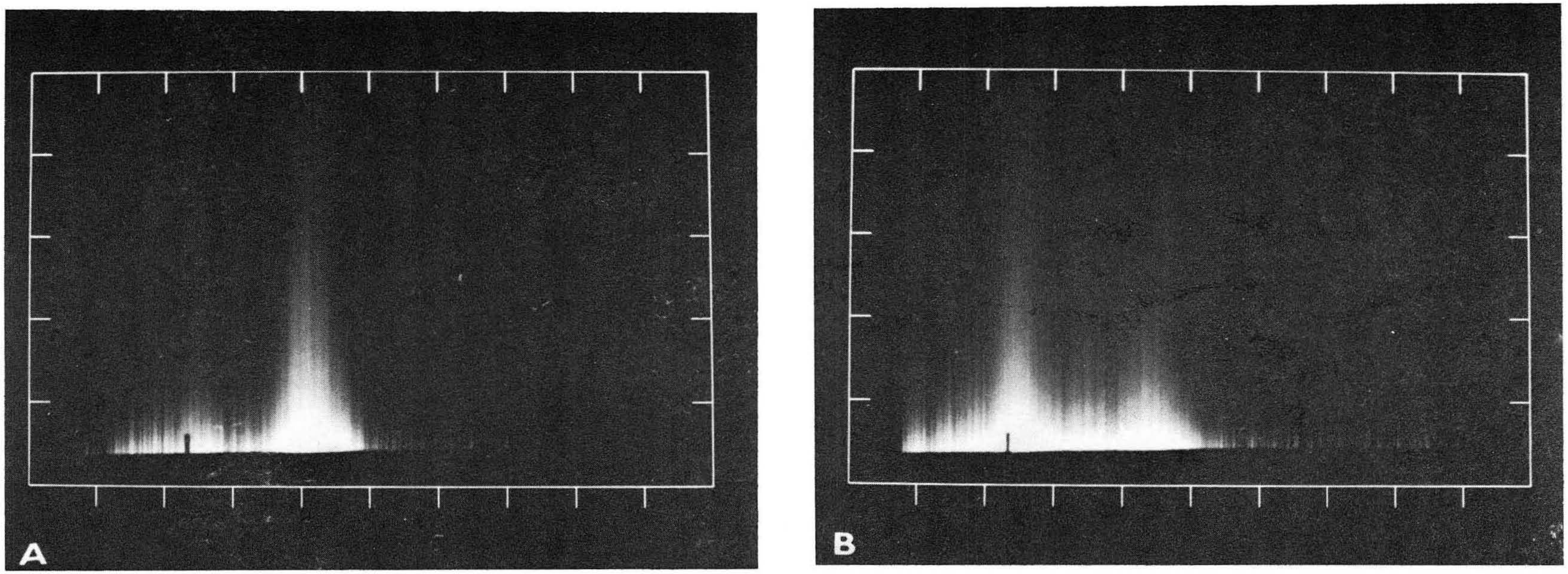

IM 2484

Fig. 4 X-ray microanalysis images showing that the precipitates are composed of Ni and Ti; (a) carbon extraction replica mounted on Ni grid, (b) on Ti grid.

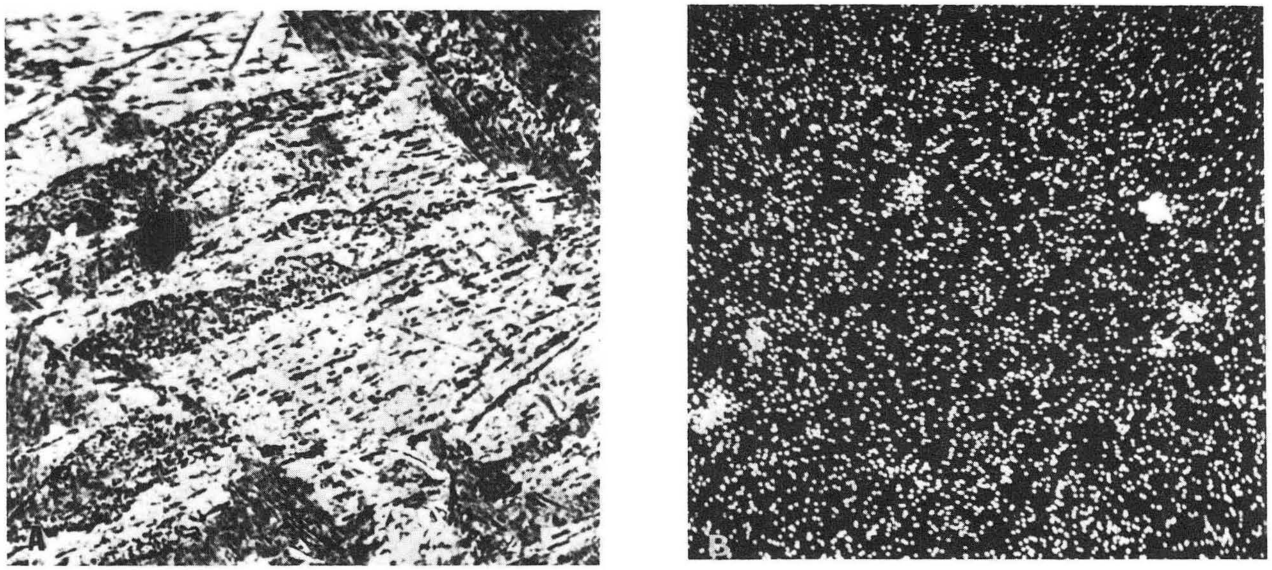

IM 2483

Fig. 5 Electron beam probe analysis; (a) optical photograph (×550), (b) x-ray image of the area using TiK_{α}.

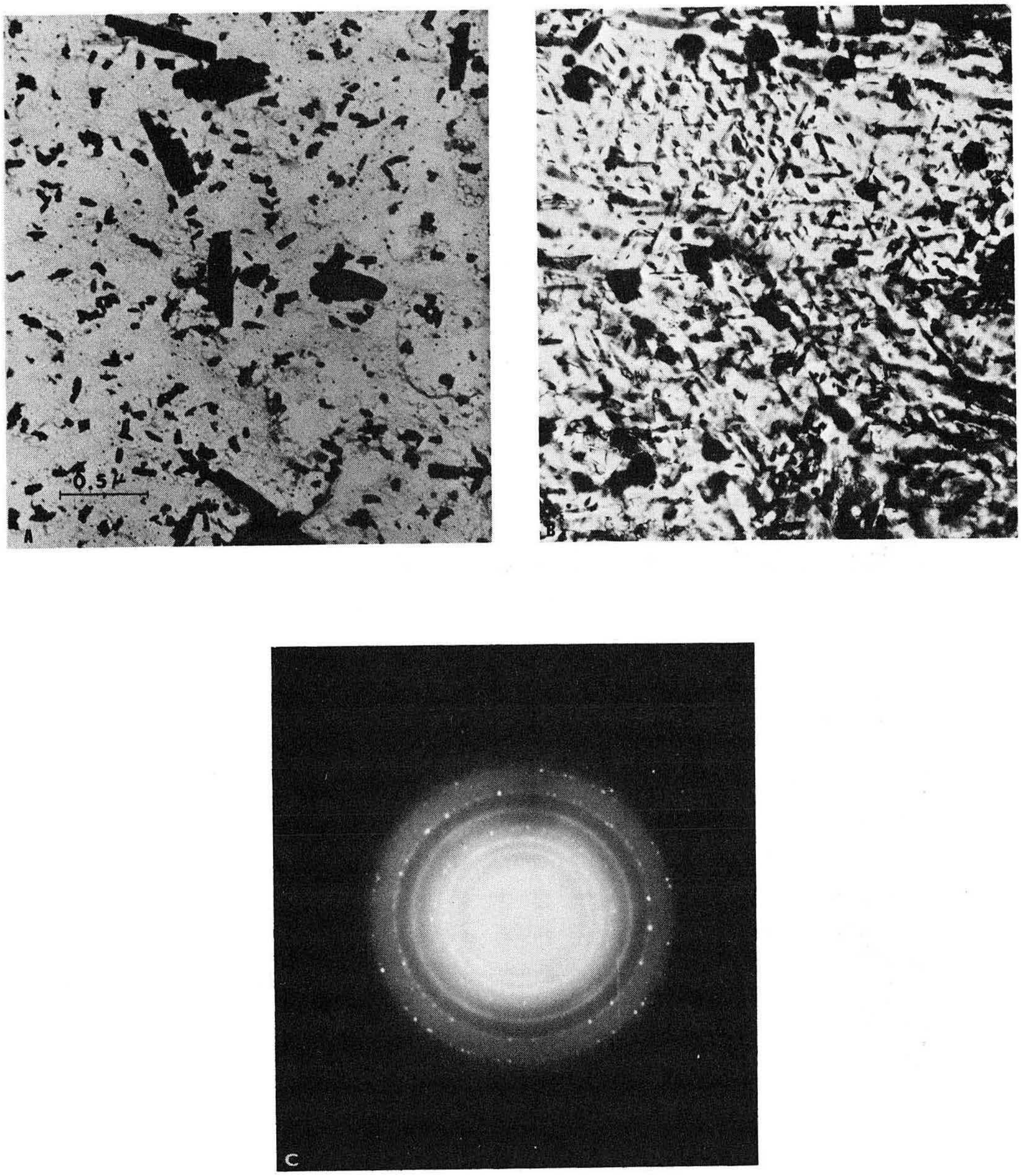

IM 2480

Fig. 6 (a) Carbon extraction replica and (b) thin foil micrograph of an overaged specimen (19-1/2 hrs aging at 600°C); (c) selected area diffraction pattern from (a).

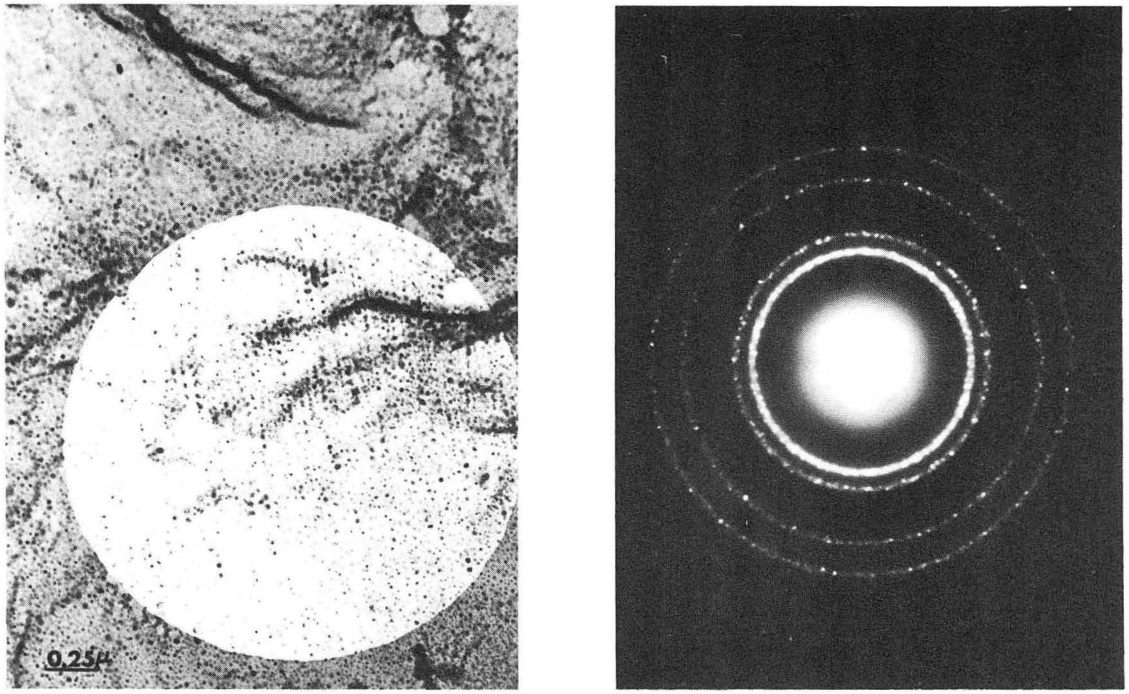

XBB 679-5307

Fig. 7 (a) Carbon extraction replica of alloy aged 19-1/2 hrs at 600°C, (b) selected area diffraction pattern from the area shown in (a). The pattern is fcc corresponding to austenite.

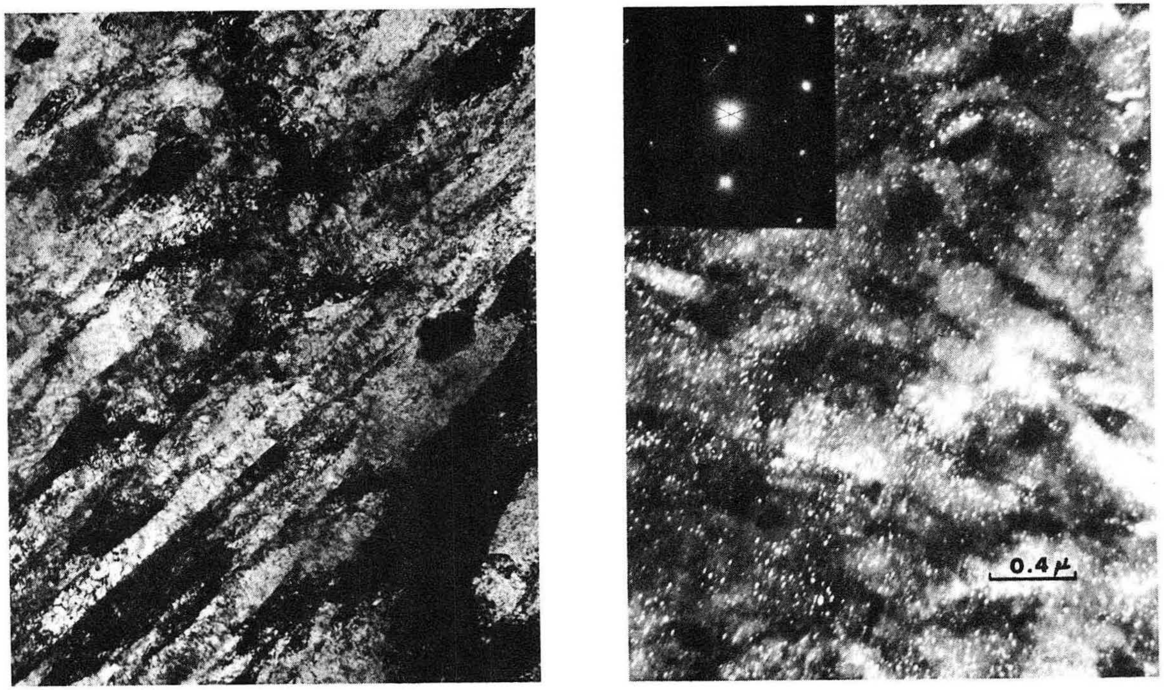

XBB 679-5309

Fig. 8 2100°F/4 hrs + LN quenched + 700°F/3 hrs aging; (a) bright field, (b) high resolution dark field of streaks (see inset) by gun tilting, reveals the precipitates.

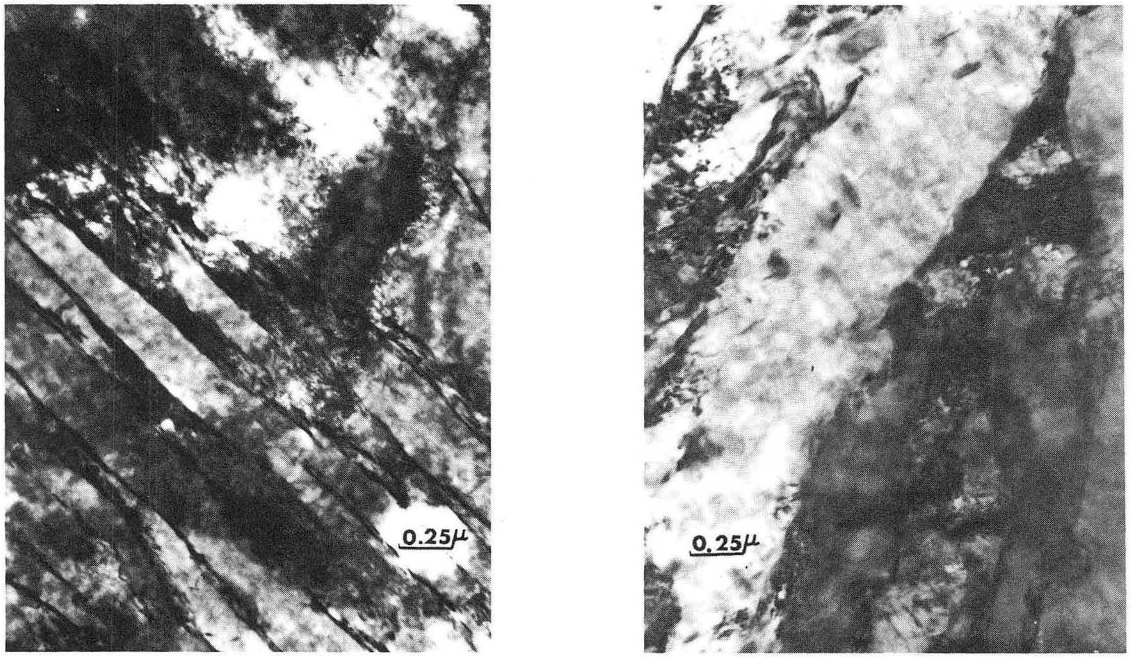

XBB 679-5308

Fig. 9 Showing sub- and grain boundary precipitation after the aging at 900°F/1 hr; (a) LN quenching, (b) air quenching.

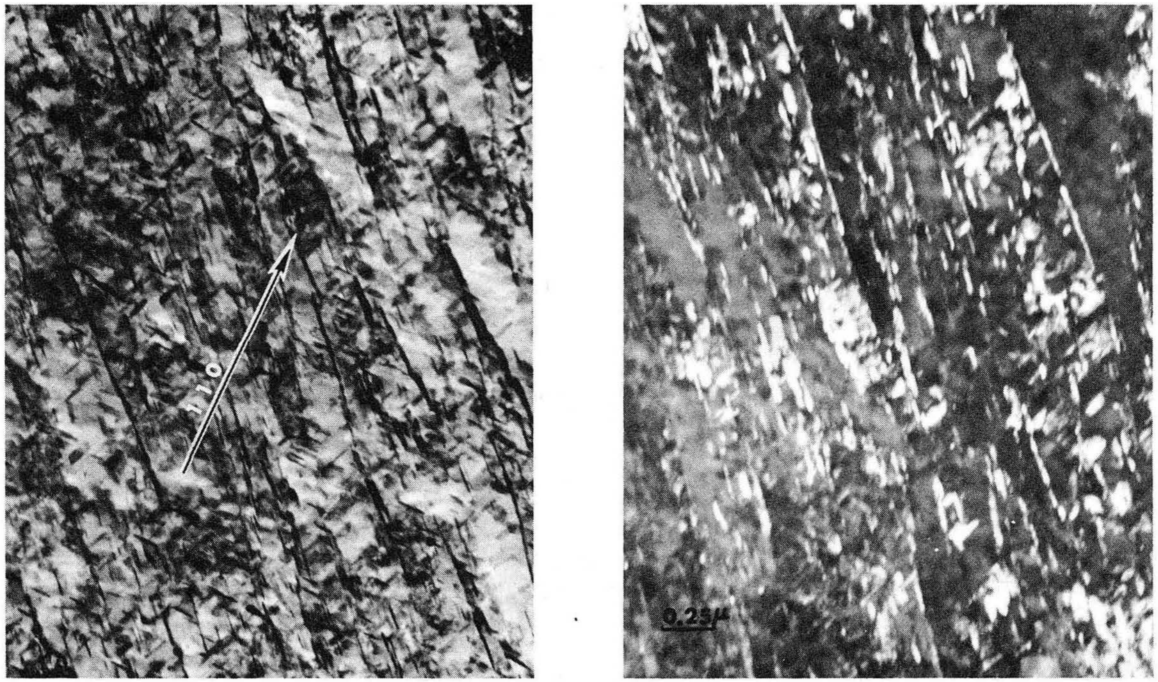

XBB 679-5310

Fig. 10 Alloy aged for 3 hrs at 900 F after LN quench. (a) Bright field, (b) gun tilt dark field (using Ni_3Ti reflections) showing both matrix and boundary precipitates of Ni_3Ti.

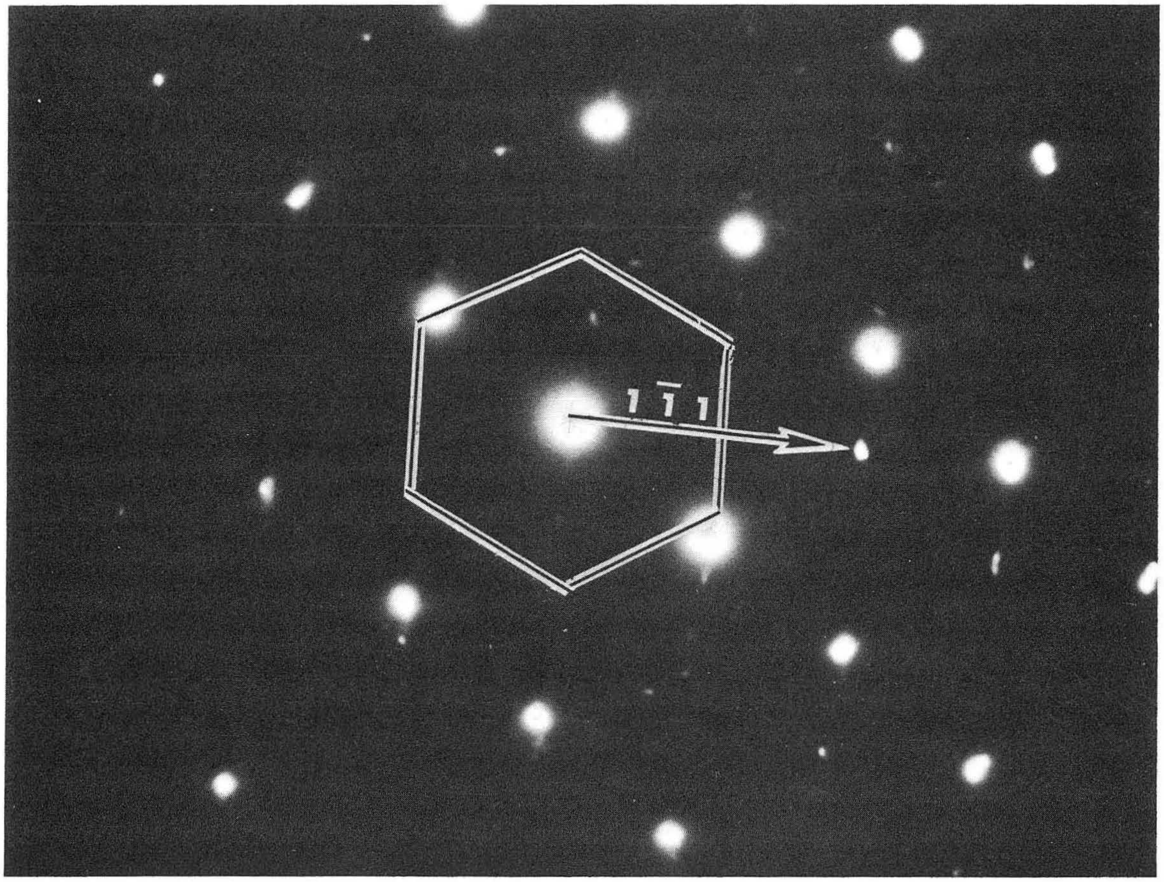

XBB 679-5305

Fig. 11 Selected area diffraction pattern from alloy similar to Fig. 10. The orientation relationships between precipitates and the matrix is $(0001)_\eta//(110)_\alpha$, $[2\bar{1}\bar{1}0]_\eta//[1\bar{1}1]_\alpha$.

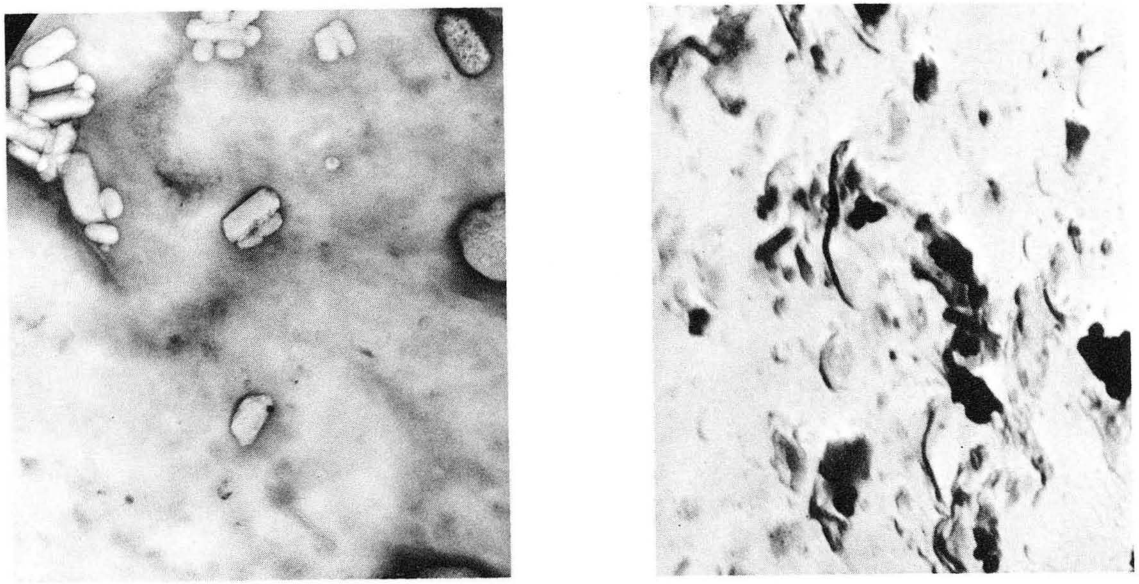

XBB 679-5311

Fig. 12 Carbon replica fractographs, (a) flat feature of brittle fractured surface which is characteristic of intergranular fracture (900°F/12 hrs aging); (b) some dimpled feature of the partially ductile fractured surface which is characteristic of transgranular fracture.

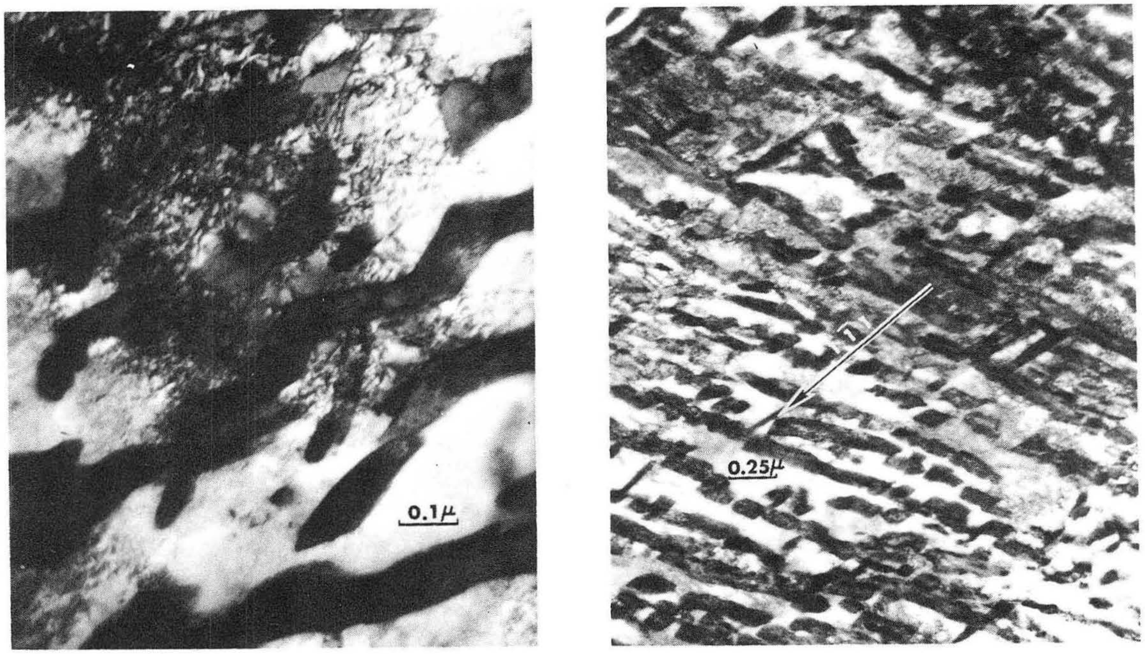

XBB 679-5306

Fig. 13 Thin foil of alloy aged 12 hrs at 900°F after 30% cold rolling. (a) Showing shearing of particles in the matrix in ⟨111⟩. (b) Showing shearing and fracture of boundary particles.